

DISSOLUTION KINETICS OF Fe₃O₄ NANOPARTICLES
IN THE ACID MEDIAIryna Tsykhanovska^{1, *}, Victoria Evlash², Alexandr Alexandrov¹, Tatyana Gontar¹<https://doi.org/10.23939/chcht13.02.170>

Abstract. The Fe₃O₄ nanoparticles dissolution in the acid media (pH = 1.8–5.0; 3 h) has been studied. The kinetic curves have been obtained and Fe₃O₄ solubility has been determined using spectrochemical, gravimetric and atomic absorption methods. Fe₃O₄ solubility was found to be increased with the increase in inorganic media acidity and the time. By means of SEM, XRD and NMR analyses the effect of acidic media on the physico-chemical properties of Fe₃O₄ particles surface has been determined.

Keywords: Fe₃O₄ nanoparticles, solubility, kinetics, acidic media.

1. Introduction

The state medical organizations investigations of many countries show that one of the scarcest microelements in the food is iron and the iron-deficient state is in the lead of alimentary disorders. The topical issue in the world is providing the daily diets with the digestible Fe(II) [1-3]. The main property of Fe₃O₄ nanoparticles is the ability to form new functional and technological characteristics of food systems: to improve the fat-emulsifying, water- and fat-retaining ability; to affect the dimensional stability, quality profile, yield and storage time of the finished product, *i.e.* Fe₃O₄ nanoparticles exhibit a complex action, which is very important in the development of new technologies, including food ones [4-6].

If physico-chemical properties of Fe₃O₄ as a magnetic material, especially in a monocrystal state, have been studied enough, no data on the properties of Fe₃O₄ as a component of Magnetofood were provided. In particular, to estimate the behavior of Fe₃O₄ magnetic nanoparticles in the aggressive environments of the gastrointestinal tract (GIT) it is important to know the following: kinetics of Fe₃O₄ solubility in the acidic media; the changes in the elemental composition of the particles

near-surface layer; the effect of medium on physicochemical properties of Fe₃O₄ nanoparticles; the changes in structural and functional parameters of Fe₃O₄, occurred under the influence of acidic media.

It should be noted that in spite of enormous amount of modifiers, food and dietary supplements, all of them have a narrow orientation and do not have a complex action [7, 8]. Recently, various compounds of iron are used for the improvement of food systems characteristics and food fortification. The most used iron compounds are sulfates, orthophosphates, pyrophosphates, fumarates, gluconates and ammonium-ferric citrates, the brown and green modification of which is known as a food additive E381. It is considered appropriate to improve the technological indices and enrich with iron a flour, flour-based food, pastas, baby food, white salt, milk and dairy products, sugar, liquid chlorophyll, cereal products, confectionery, cheese, rice, instant coffee, and dry mashed potatoes [9–28].

However, according to the literary data [10-15, 20-22], the food fortification with iron salts can lead to the lipids oxidation and strange taste. The introduction of iron sulphate to milk and milk products promotes the heat-resistance of lipases but debases their organoleptic properties [16, 17, 25-27]. An addition of iron mineral salts to the dry mashed potatoes results in the appearance of grey-green color of the product [8, 12, 22, 28].

Therefore, the studies on creation of new modifiers, food and dietary iron-containing supplements of complex action are of topical issue. Their introduction to various food systems allows to create the quality assortment of the functional food. For this purpose we suggest nanopowder Fe₃O₄ as a basic component of Magnetofood additive. Fe₃O₄ nanoparticles have a large specific surface, high activity and such properties as biological compatibility with living organisms, affinity to proteins and carbohydrates, bacteriostatic action, high thermal stability. Fe₃O₄ in food systems shows the reducing, antioxidant, sorption, complex forming, fat-emulsifying, moisture-binding, fat- and moisture-retaining properties, and also can act as an additional source of digestible iron Fe²⁺ [4–6].

The aim of this research is to study dissolution kinetics of Fe₃O₄ nanoparticles in the acid medium and

¹ Ukrainian Engineering Pedagogic Academy,
16, Universitetskaya St., 61003 Kharkiv, Ukraine

² Kharkiv State University of Food Technology and Trade,
333, Klochkovskaya St., 61051 Kharkiv, Ukraine

* cikhanovskaja@gmail.com

© Tsykhanovska I., Evlash V., Alexandrov A., Gontar T., 2019

changes in physico-chemical state of nanoparticles surface under the influence of pH 1.8–5.0 medium.

2. Experimental

2.1. Investigation of Dissolution Kinetics of Fe₃O₄ Nanoparticles in the Acid Media of Different pH

The dissolution kinetics of Fe₃O₄ nanoparticles was studied using a black color high-dispersive powder of Fe₃O₄ with the particles size of ~78 nm. The samples were obtained according to the technology developed by us [29, 30] *via* the reaction of chemical condensation (co-precipitation) of the iron salts in an alkaline medium.

The kinetics was studied in the acid media of different pH values corresponding to the model conditions of biomedical experiment [31]: the experiment temperature 310 K; *stomach*: pH 1.8–2.0, digestive fluid amount 20–150 ml, residence time 60 min; *duodenum*: pH 4.5–5.0, digestive fluid amount 30–70 ml, residence time 30 min.

Fe₃O₄ was dissolved using an impeller mixer. The initial solutions of pH = 1.8–5.0 were prepared according to the literature data [31]. To simulate the stomach conditions the value of pH 1.8 was provided by 0.2 M solution of chloride acid and gastric juice with pepsin enzyme. For simulating the duodenum conditions the pH value of 5.0 was provided by 0.2 M HCl and digestive juice prepared by mixing 0.2 M HCl with pancreatin (0.1 wt %), gastric juice (0.1 wt %) and bile (0.1 wt %).

Fe₃O₄ (2.5 g) was added to the initial solutions and the resulting mixtures were kept in a thermostat at 310 K for 180 min under constant stirring (100 rpm). Every 30 min the samples for the analysis (10 ml) were taken and the same volume of initial solution was added.

The value of pH was controlled with a glass electrode EVL 61-03 and an universal ionomer EV-74.

The concentrated nitric acid (7 drops of HNO₃(conc.) per 10 ml of the sample) was added for complete oxidation of Fe²⁺ to Fe³⁺ and the resulting solution was

boiled for 1–2 min. Then the samples were cooled to 293 K and the excess acid was neutralized with a sodium hydrogen carbonate.

In the investigated samples of acidic solutions we determined Fe(III) concentration *via* spectrophotometric method using a photocolormeter KFK-2-UHL with a light wavelength of 490 nm; Fe_(total) *via* gravimetry and atomic-absorption spectroscopy using a Saturn spectrophotometer with atomization in an air-acetylene flame (pressure 0.2 MPa, flame temperature 2523 K, wavelength for Fe 248.3 nm). Then the calibration curve method was applied (Fig. 1). The graph was plotted within the range of Fe³⁺ and Fe_(total) measured concentrations by using the standard solutions of FeCl₃ (0.10 mg/cm³ in 0.1M HCl).

To compare the physico-chemical methods we applied a mathematical treatment of the analytical results according to Student's *t*-test (Eqs. (4)–(12)) [32].

To determine the order and rate constant of Fe₃O₄ dissolution reaction the graphical method was used according to Eqs. (13)–(16) [32].

2.2. The Effect of Acid Medium on Physico-Chemical State of Fe₃O₄ Particles Surface

To determine the effect of acid medium on the Fe₃O₄ near-surface layer and the structural changes, the SEM, XRD and NMR methods were used.

Different samples of Fe₃O₄ particles (finely dispersed ones – samples 1 and 2 and monocrystalline (MCS) ones – samples 3 and 4) prepared by different technologies were used (Table 1).

The Fe₃O₄ nanoparticles size in the sample 1 was determined using a scanning electron microscope JSM-820 (JEOL) with the magnification of 150000. The obtained images were processed using AutoCAD 2004 and MathCad 2007. The distribution of Fe₃O₄ nanoparticles in the sample 1 was calculated according to the diameter. The number of particles to determine the average values was not less than 500.

Table 1

Characteristics of Fe₃O₄ samples

Experimental samples	<i>d</i> , nm	Technology
Sample 1	8	Synthesis <i>via</i> chemical co-precipitation (condensation); Initial sample – sample 1
Sample 2	8	Treatment of sample 1 (<i>T</i> = 310 K, <i>t</i> = 60 min) with HCl solution (pH = 1.8)
Sample 3	MCS*	Monocrystalline sample (MCS); Initial sample – sample 3
Sample 4	MCS	Treatment of sample 3 (<i>T</i> = 310 K, <i>t</i> = 60 min) with HCl solution (pH = 1.8)

Note: *MCS is a monocrystalline Fe₃O₄ sample, obtained by the high-temperature growth from the gas phase at the General Physics Department of the Physics Faculty of Kharkiv National University under the guidance of Prof. S. Kuntsevich

X-ray phase analysis of the experimental sample 1 was done on Semens D500 powder diffractometer (Germany) in copper radiation with a graphite monochromator. The studies were carried out by the well-known Bragg-Brenton technique [33]. 0.5 cm³ of the sample 1 dried at room temperature (293 K) was used for the analysis. The sample was thoroughly ground and mixed in a mortar, and then transferred to a glass cuvette with a working volume of 2 × 1 × 0.1 mm³ to register the diffractogram. The full-profile XRD pattern was measured in the angular interval 10° < 2θ < 150° with 0.02 step and the accumulation time of 12 s at each point. The primary phase search was performed using a PDF-4 file [34], after which the XRD analysis was performed using the Ritveld method.

The average size of Fe₃O₄ nanoparticles in the sample 1 was determined by Eq. (17) using the Scherrer equation [35].

To determine the elemental composition of Fe₃O₄ nanoparticles in the samples 1 and 2, a scanning electron microscope JSM-820 (JEOL) with EDX connector was used. X-ray spectra were obtained under electron bombardment of Fe₃O₄ samples using an acceleration voltage of 20 kV (according to the characteristic spectral lines of iron and oxygen). The elemental compositions were determined through the analysis of the characteristic X-rays from the volume and surface of Fe₃O₄ nanoparticles.

NMR researches on ⁵⁷Fe nuclei were carried out for the samples 1, 2 (finely dispersed nanoparticles with the size of ~78 nm) and samples 3, 4 (monocrystalline samples) at 298 K on a Tecmag Redstone spectrometer (1–500 MHz). An ordinary iron powder (⁵⁷Fe standard) with the particles size of 150 μm was used for the comparison. Fe₃O₄ samples and a reference sample (⁵⁷Fe standard) had a natural content of ⁵⁷Fe isotope. The samples 2 and 4 were kept in a hydrochloric acid solution (pH = 1.8) at 310 K for 60 min, then washed with distilled water and dried at 298 K for 25–30 min. 20 mg of the analyzed sample was thoroughly ground and mixed in a mortar, and then transferred to the ampoule with a working volume of 15 cm³ and diameter of 5 mm. Another ampoule was loaded with 20 mg of the reference sample (⁵⁷Fe).

3. Results and Discussion

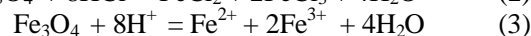
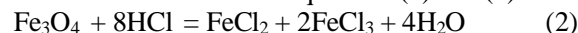
3.1. Investigation of Dissolution Kinetics of Fe₃O₄ Nanoparticles in the Acid Media of Different pH

Fe₃O₄ nanoparticles of the experimental sample were synthesized from the aqueous solution of Fe(II) and Fe(III) salts in the alkaline medium according to Eq. (1):



To create an alkaline medium (pH = 10–11) the 25% ammonium hydroxide solution was used. The initial Fe(III) chloride and Fe(II) sulfate were used in a stoichiometric ratio with 1.75 excess of Fe(II) salt. For all cases, the synthesis was carried out using the same algorithm: the excess of 25% ammonium hydroxide solution is added by thread to the filtered 10% solution of Fe(II) and Fe(III) salts under slow stirring at the temperature of 323–333 K. A precipitate of black color and the temperature increase by 7–8 K are immediately observed. After 1 hour the heating is turned off and the stirring is continued until the mixture is cooled. Then the reaction mixture is kept in a constant MF for 12 h to separate Fe₃O₄ and saline solution till the precipitate maturation. After this, the solution is repeatedly washed using magnetic decantation to pH = 9–10 [30, 31].

Next stage was the investigation of Fe₃O₄ dissolution kinetics in the acid media (pH = 1.8–5.0). The process is based on the reaction equations (2) and (3):



The concentration of iron in ionic and atomic states in acidic solutions was determined by means of calibration curves (Fig. 1).

It should be noted that the atomic-absorption method of the quantitative analysis was chosen for Fe(III) or Fe_(total) due to its high sensitivity. It provides sufficiently low limits for the elements determination (10⁻⁶–10⁻⁷%) and gives high accuracy within 1–4% with a sensitivity of 0.001 mg/cm³. Moreover, a small quantity of investigated solutions is needed.

For the more complete and accurate evaluation of Fe₃O₄ solubility and determination of Fe³⁺ or Fe_(total) concentrations we also used the gravimetric method, in addition to the spectrophotometry and atomic-absorption method. The essence of the method is the precise measurement of Fe₃O₄ weight which is non-dissolved after being in the acid medium.

The investigating results of the Fe₃O₄ solubility in different acid media according to the concentration of Fe²⁺ and Fe³⁺ ions are given in Tables 2 and 3, respectively.

Figs. 2 and 3 show the kinetic curves of Fe₃O₄ solubility in acid media which were plotted as Fe³⁺ concentrations vs. dissolution time.

Analysis of the experimental data (Tables 2–3, Figs. 2–3) shows the best solubility of Fe₃O₄ sample in acid medium with pH = 1.8. The decrease in acidity to pH = 5.0 degrades the solubility by 97.0% for 180 min. In all cases the tendency of solubility increase with the increase in dissolution time of Fe₃O₄ nanoparticles in the acid medium preserves. At pH = 1.8 for 180 min the solubility increases for Fe²⁺ – by 2.04 times and for Fe³⁺ – by 1.83 times; at pH = 5.0 the increase is by 2.75 times for

Fe²⁺ and by 2.43 times – for Fe³⁺. Hence, the concentrations of Fe²⁺ and Fe³⁺ cations transferred into the solution do not correspond to the stoichiometry of Fe₃O₄. It means that the near-surface layer of nanoparticles, the structural defectiveness of which is demonstrated in [36, 37], is stripped under the influence of an acid medium. The maximum concentrations of Fe²⁺ and Fe³⁺ cations observed in the solutions of pH = 1.8 correspond to the

value of gastric juices after staying of Fe₃O₄ particles in them for 180 min: $C_{(Fe^{2+})} = (3.5 \cdot 10^{-3}) - (3.7 \cdot 10^{-3}) \text{ mol/dm}^3$; $C_{(Fe^{3+})} = C_{(Fe^{(total)})} = (6.2 \cdot 10^{-3}) - (6.4 \cdot 10^{-3}) \text{ mol/dm}^3$. The concentrations of Fe²⁺ and Fe³⁺ cations in the medium of pH = 5.0 for the same time are:

$$C_{(Fe^{2+})} = (1.0 \cdot 10^{-4}) - (1.1 \cdot 10^{-4}) \text{ mol/dm}^3$$

$$C_{(Fe^{3+})} = C_{(Fe^{(total)})} = (1.5 \cdot 10^{-4}) - (1.7 \cdot 10^{-4}) \text{ mol/dm}^3$$

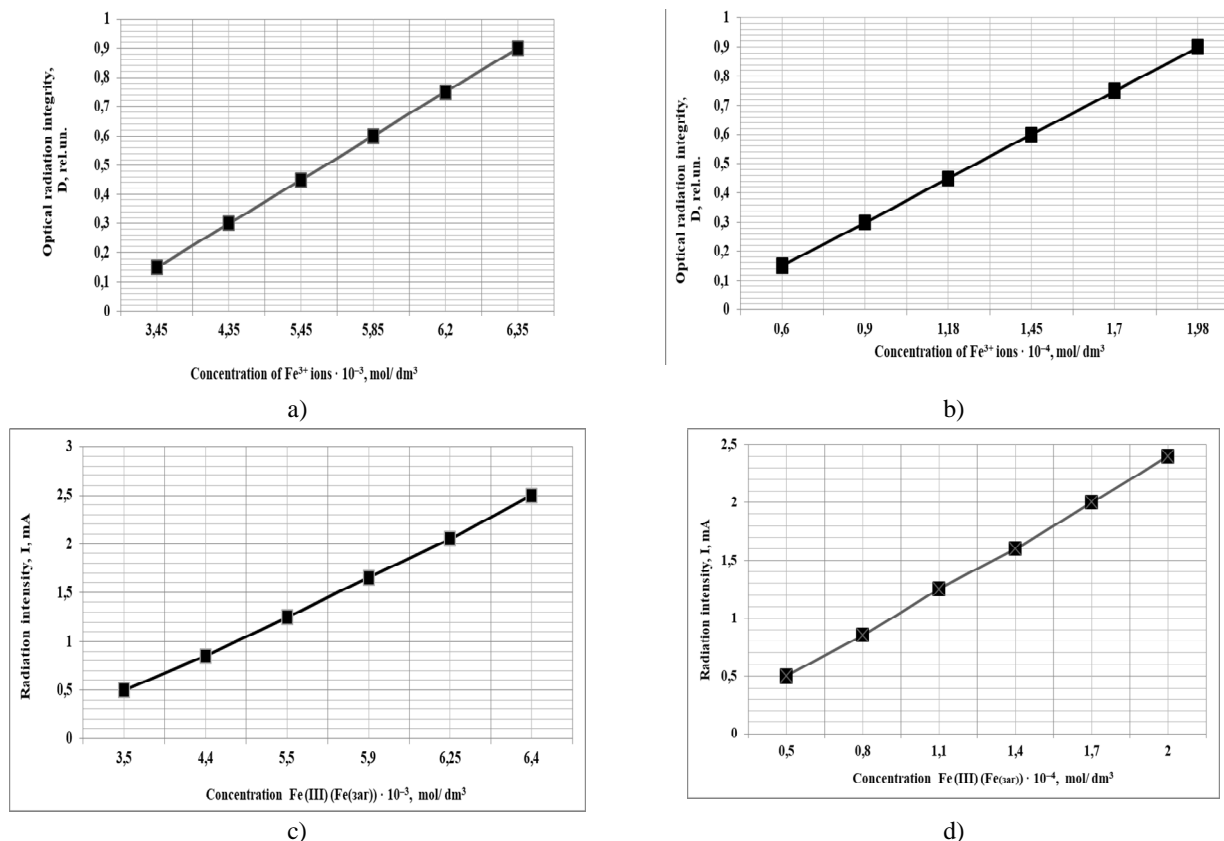


Fig. 1. Calibration curves for the determination of Fe³⁺ and Fe(III) (Fe_{total}) concentrations by spectrophotometric method at pH 1.8 (a) and pH 5.0 (b); and atomic-adsorption method at pH 1.8 (c) and pH 5.0

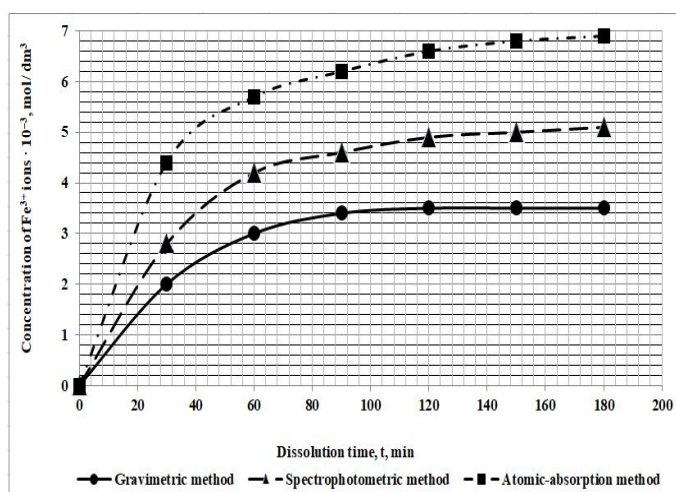
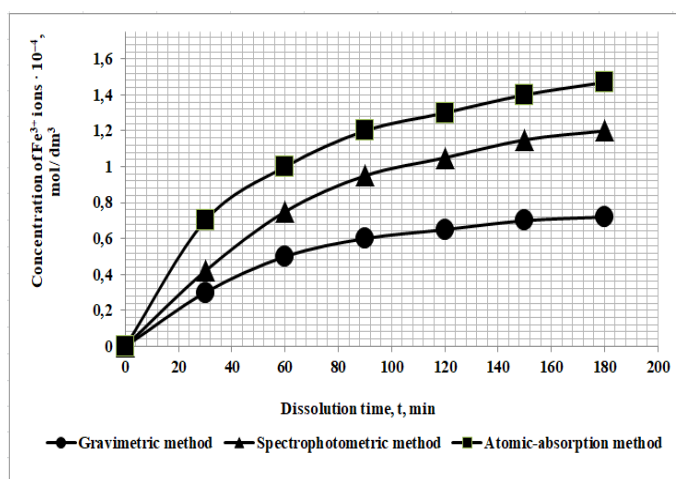
Table 2

Fe₃O₄ solubility in different acid media (according to the concentration of Fe²⁺ ions)

Dissolution time, min	Solution pH	Concentration of Fe ²⁺ , mol/dm ³		
		Spectrophotometric method	Atomic-absorption method	Gravimetric method
30	1.8	$1.75 \cdot 10^{-3}$	$1.80 \cdot 10^{-3}$	$1.60 \cdot 10^{-3}$
60	1.8	$2.35 \cdot 10^{-3}$	$2.40 \cdot 10^{-3}$	$2.20 \cdot 10^{-3}$
90	1.8	$2.90 \cdot 10^{-3}$	$2.95 \cdot 10^{-3}$	$2.75 \cdot 10^{-3}$
120	1.8	$3.15 \cdot 10^{-3}$	$3.20 \cdot 10^{-3}$	$3.00 \cdot 10^{-3}$
150	1.8	$3.35 \cdot 10^{-3}$	$3.45 \cdot 10^{-3}$	$3.25 \cdot 10^{-3}$
180	1.8	$3.65 \cdot 10^{-3}$	$3.70 \cdot 10^{-3}$	$3.50 \cdot 10^{-3}$
30	5.0	$0.35 \cdot 10^{-4}$	$0.40 \cdot 10^{-4}$	$0.30 \cdot 10^{-4}$
60	5.0	$0.60 \cdot 10^{-4}$	$0.65 \cdot 10^{-4}$	$0.55 \cdot 10^{-4}$
90	5.0	$0.70 \cdot 10^{-4}$	$0.75 \cdot 10^{-4}$	$0.65 \cdot 10^{-4}$
120	5.0	$0.80 \cdot 10^{-4}$	$0.85 \cdot 10^{-4}$	$0.75 \cdot 10^{-4}$
150	5.0	$0.90 \cdot 10^{-4}$	$0.95 \cdot 10^{-4}$	$0.85 \cdot 10^{-4}$
180	5.0	$1.05 \cdot 10^{-4}$	$1.10 \cdot 10^{-4}$	$1.00 \cdot 10^{-4}$

Fe₃O₄ solubility in different acid media (according to the concentration of Fe³⁺ ions)

Dissolution time, min	Solution pH	Concentration of Fe ³⁺ , mol/dm ³		
		Spectrophotometric method	Atomic-absorption method	Gravimetric method
30	1.8	$3.45 \cdot 10^{-3}$	$3.50 \cdot 10^{-3}$	$3.30 \cdot 10^{-3}$
60	1.8	$4.35 \cdot 10^{-3}$	$4.40 \cdot 10^{-3}$	$4.20 \cdot 10^{-3}$
90	1.8	$5.45 \cdot 10^{-3}$	$5.50 \cdot 10^{-3}$	$5.30 \cdot 10^{-3}$
120	1.8	$5.85 \cdot 10^{-3}$	$5.90 \cdot 10^{-3}$	$5.70 \cdot 10^{-3}$
150	1.8	$6.20 \cdot 10^{-3}$	$6.25 \cdot 10^{-3}$	$6.05 \cdot 10^{-3}$
180	1.8	$6.35 \cdot 10^{-3}$	$6.40 \cdot 10^{-3}$	$6.20 \cdot 10^{-3}$
30	5.0	$0.65 \cdot 10^{-4}$	$0.70 \cdot 10^{-4}$	$0.50 \cdot 10^{-4}$
60	5.0	$1.10 \cdot 10^{-4}$	$1.15 \cdot 10^{-4}$	$0.95 \cdot 10^{-4}$
90	5.0	$1.30 \cdot 10^{-4}$	$1.35 \cdot 10^{-4}$	$1.15 \cdot 10^{-4}$
120	5.0	$1.40 \cdot 10^{-4}$	$1.45 \cdot 10^{-4}$	$1.25 \cdot 10^{-4}$
150	5.0	$1.55 \cdot 10^{-4}$	$1.60 \cdot 10^{-4}$	$1.40 \cdot 10^{-4}$
180	5.0	$1.65 \cdot 10^{-4}$	$1.70 \cdot 10^{-4}$	$1.50 \cdot 10^{-4}$

**Fig. 2.** Kinetic curves of the Fe₃O₄ solubility in acid medium (pH = 1.8) obtained *via* different physico-chemical methods**Fig. 3.** Kinetic curves of Fe₃O₄ solubility in acid medium (pH = 5.0) obtained *via* different physico-chemical methods

The best solubility of Fe₃O₄ nanoparticles was observed during the first 90 minutes of the study (Figs. 2-3). Then, the value did not significantly change. The mass fraction of Fe₃O₄ sample, which passes into the model solutions of pH = 1.8 and pH = 5.0, is 14.3 and 0.4 %, respectively. In general $w = 14.7$ % or the mass fraction of the sample, that passes into the ionic state during the staying in the acid media cannot cause the toxic effects, since it does not exceed the threshold limit value (TLV) [38] and can be considered as an additional source of the microelement of Fe for the prevention of iron deficiency anemia.

When using Fe₃O₄ nanoparticles in the food industry, their partial dissolution in the acid medium of the stomach is possible with the formation of toxic iron salts. The results of the maximum Fe₃O₄ particles solubility (Tables 2-3, Figs. 2-3) were compared with the permissible concentrations of iron cations [38]. The TLV value for Fe³⁺ is $3.57 \cdot 10^{-4}$ mol/kg. The maximum concentration of iron cations, which passed into a solution, was observed after 180 min and was calculated in terms of the average weight of a person. In the acid media of pH = 1.8 and pH = 5.0 it is equal to $8.53 \cdot 10^{-5}$ and $2.27 \cdot 10^{-6}$ mol/kg, respectively.

In the acid media (pH = 1.8–5.0) with the increase in time of Fe₃O₄ particles processing by HCl solution, we observe the increase in Fe²⁺ and Fe³⁺ cations concentration in the solution (Tables 2-3, Figs. 2-3). The maximum value of the Fe₃O₄ dissolution degree was observed after three hours in a medium with pH = 1.8. There were no significant changes with further dissolution.

The solubility of the finely dispersed Fe₃O₄ powder is caused by a small size of its particles (~78 nm), the structure of the crystal lattice and ability to be solvated by H₂O molecules, contributing to iron transition into the ionic state (Fe²⁺ and Fe³⁺) during staying of Fe₃O₄ particles in acidic media. The increase in nanoparticles solubility with increasing time is associated with in-depth proceeding of complexation and solvation physico-chemical processes [5].

To compare the physico-chemical methods used to analyze the Fe₃O₄ dissolution process, the results of the analytical determinations were mathematically processed via the Student's *t*-test according to Eqs. (4)–(12) [32].

At first, the average number (\bar{x}) of the experimental concentration values of iron cations was found according to Eq. (4):

$$\bar{x} = \frac{\sum x_i}{n} \quad (4)$$

where n is a number of measurements, $n = 5$.

We compared each of the results (x_i), and found deviations from the arithmetic mean according to Eq. (5):

$$d_i = x_i - \bar{x} \quad (5)$$

These deviations characterize the definition error. Then we found the average deviation d_{av} by Eq. (6):

$$d_{av} = \frac{\sum(x_i - \bar{x})}{n} = \frac{\sum d_i}{n} \quad (6)$$

Obviously, the less the value of d_{av} , the more precisely the measurement, *i.e.*, the less the result which is distorted by random errors. The standard deviation was calculated according to Eq. (7):

$$S^2 = \frac{\sum d_i^2}{n-1} \quad (7)$$

The standard deviation of the arithmetic mean (the square root of the variance) calculated from formulas (8) and (9) is of the particular interest:

$$S = \sqrt{S^2} \quad (8)$$

$$S_{\bar{x}} = \frac{S}{\sqrt{n}} \quad (9)$$

To determine the accuracy of the direct measurement of A (confidence interval), the reliability value of α (percentage of cases) was specified. Usually in the analytical measurements $\alpha = 0.95$ or 0.99 , which means that 95 or 99 % of all measurements are within certain limits determined by the formula (10):

$$A_{a,K} = S_{\bar{x}} \cdot t_{a,K} \quad (10)$$

The normalized deviation coefficient or Student's criterion was found from the tabular data depending on α and K (the number of free degrees). $K = n - 1$. The coefficients are given in Table 4 [32].

The value of confidence limits, within which every determined value of x_i can be determined, is calculated according to Eq. (11):

$$x_i = \bar{x} \pm A_{a,K} \quad (11)$$

Table 4

Normalized deviation coefficients

K/α	2	3	4	5	6	7	8	9	10
0.95	4.30	3.18	2.78	2.57	2.45	2.37	2.31	2.26	2.23
0.99	9.93	5.84	4.60	4.03	3.71	3.50	3.36	3.25	3.17

Table 5

Determination of Fe³⁺ cations concentration in the model solution of pH = 1.8 via the spectrophotometric method

x_i	\bar{x}	d_i	d_{av}	d_i^2	S^2	S	$S\bar{x}$	$A_{a,K}$	A_{rel}
$5.45 \cdot 10^{-3}$	$5.4 \cdot 10^{-3}$	$-0.05 \cdot 10^{-3}$	$0.044 \cdot 10^{-3}$	$0.0025 \cdot 10^{-6}$	$0.00325 \cdot 10^{-6}$	$0.18 \cdot 10^{-3}$	$0.08 \cdot 10^{-3}$	$0.17 \cdot 10^{-3}$	3.00%
$5.35 \cdot 10^{-3}$		$0.05 \cdot 10^{-3}$		$0.0025 \cdot 10^{-6}$					
$5.40 \cdot 10^{-3}$		0		0					
$5.45 \cdot 10^{-3}$		$-0.05 \cdot 10^{-3}$		$0.0025 \cdot 10^{-6}$					
$5.35 \cdot 10^{-3}$		$0.05 \cdot 10^{-3}$		$0.0025 \cdot 10^{-6}$					

Table 6

Determination of Fe³⁺ cations concentration in the model solution of pH = 1.8 via the atomic-absorption method

x_i	\bar{x}	d_i	d_{av}	d_i^2	S^2	S	$S\bar{x}$	$A_{a,K}$	A_{rel}
$5.5 \cdot 10^{-3}$	$5.52 \cdot 10^{-3}$	$0.02 \cdot 10^{-3}$	$0.04 \cdot 10^{-3}$	$0.0004 \cdot 10^{-6}$	$0.0025 \cdot 10^{-6}$	$0.05 \cdot 10^{-3}$	$0.022 \cdot 10^{-3}$	$0.11 \cdot 10^{-3}$	2.19%
$5.55 \cdot 10^{-3}$		$-0.03 \cdot 10^{-3}$		$0.0009 \cdot 10^{-6}$					
$5.45 \cdot 10^{-3}$		$0.07 \cdot 10^{-3}$		$0.0049 \cdot 10^{-6}$					
$5.5 \cdot 10^{-3}$		$0.02 \cdot 10^{-3}$		$0.0004 \cdot 10^{-6}$					
$5.6 \cdot 10^{-3}$		$-0.08 \cdot 10^{-3}$		$0.0064 \cdot 10^{-6}$					

Table 7

Determination of Fe³⁺ cations concentration in the model solution of pH = 1.8 via the gravimetric method

x_i	\bar{x}	d_i	d_{av}	d_i^2	S^2	S	$S\bar{x}$	$A_{a,K}$	A_{rel}
$5.3 \cdot 10^{-3}$	$5.28 \cdot 10^{-3}$	$-0.02 \cdot 10^{-3}$	$0.045 \cdot 10^{-3}$	$0.0004 \cdot 10^{-6}$	$0.0325 \cdot 10^{-6}$	$0.18 \cdot 10^{-3}$	$0.08 \cdot 10^{-3}$	$0.2 \cdot 10^{-3}$	3.80%
$5.35 \cdot 10^{-3}$		$-0.07 \cdot 10^{-3}$		$0.0049 \cdot 10^{-6}$					
$5.3 \cdot 10^{-3}$		$-0.02 \cdot 10^{-3}$		$0.0004 \cdot 10^{-6}$					
$5.2 \cdot 10^{-3}$		$0.08 \cdot 10^{-3}$		$0.0064 \cdot 10^{-6}$					
$5.25 \cdot 10^{-3}$		$0.03 \cdot 10^{-3}$		$0.0009 \cdot 10^{-6}$					

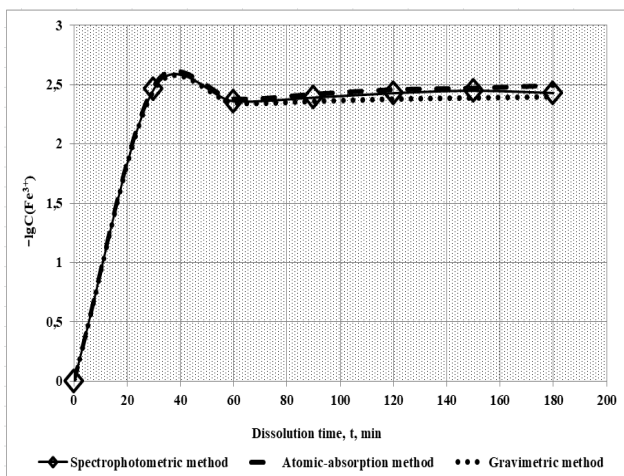


Fig. 4. The kinetic curves of the Fe₃O₄ nanoparticles dissolution in the medium of pH = 1.8

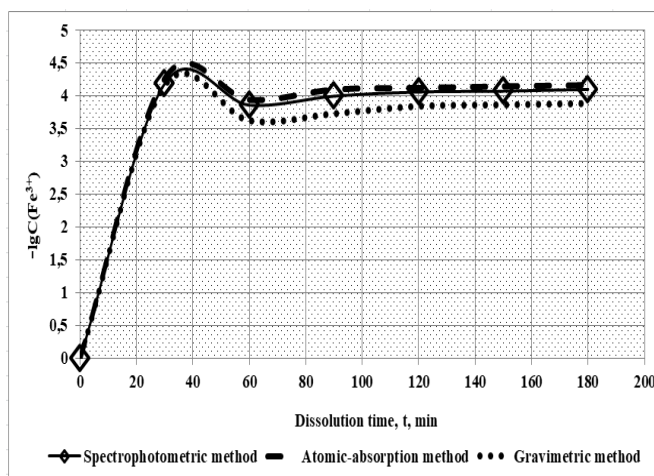


Fig. 5. The kinetic curves of the Fe₃O₄ nanoparticles dissolution in the medium of pH = 5.0

The obtained values of $A_{\alpha,K}$, and S characterize the adequacy of analysis. According to the absolute error of the arithmetic average $A_{\alpha,K}$ the relative error A_{rel} was calculated in %:

$$A_{rel} = \frac{A_{\alpha,K}}{\bar{x}} \cdot 100 \quad (12)$$

The results of statistical processing of experimental data are presented in Tables 5-7.

The results of Tables 5-7 show the advantages of the atomic-absorption method compared with spectrophotometric and gravimetric ones. This is explained by the fact that iron is binded into the colloidal systems during determination *via* spectrophotometric method and the insoluble iron compounds are formed when Fe³⁺ concentration is determined *via* the gravimetric method. To determine the order and the reaction rate constant of the Fe₃O₄ nanoparticles dissolution in the acid medium (Eqs. (2) and (3)) the kinetic curves of $\lg C_{(Fe^{3+})} = f(t)$ were plotted (Figs. 4-5) according to the graphical method [32].

It is evident that the kinetic curves consist of two linear intervals with different slopes indicating that they describe the kinetic reactions of the first order and different rates and mechanisms of the dissolution process. Apparently, different mechanisms of the Fe₃O₄ nanoparticles dissolution are specified by the size, shape and state of the particles surface.

The first mechanism is characterized by the first linear interval on the kinetic curves, a steep slope and a high rate. The reason is the dissolution of the near-surface defective and irregular layer of Fe₃O₄ nanoparticles. As a result, the surface area of the nanoparticles that interacts with the acid solution is greater and therefore the dissolution rate is higher compared with the second interval of the kinetic curves.

The second mechanism is conditioned by the dissolution of particles bottom layer and is characterized by a second interval on the kinetic curves, a flat slope and a low rate. This is due to the facts that during dissolution the irregularity of the particles surface becomes smoothed out, the nanoparticle takes the spherical-like shape and the interaction area with the acid medium decreases.

The kinetic equation of the first order reaction in the differential form is as follows:

$$V = -\frac{dC}{dt} = k \cdot C \quad (13)$$

After the separation of variables: $\frac{dc}{c} = kdt$ and integration in the range from C_0 to C and, respectively, from $t_0 = 0$ to $t = \int_{c_0}^c \frac{dC}{dt} = \int_{t_0}^t k(I)dt$ we obtain the kinetic equation of the first order reaction in the integral form (14):

$$k = \frac{2.3}{t} \lg \left(\frac{C_0}{C} \right) \quad (14)$$

where k is a reaction rate constant – a value that does not depend on the concentration of the reactants (depends on the temperature and the presence of the catalyst); C_0 is an initial concentration of the reactant at time $t_0 = 0$ (in our case $C_0 = 0$); C is the concentration of the reactant at time t ; 2.3 is a conversion factor from the natural logarithm to the decimal one ($\ln = 2.3 \lg$).

If the kinetic equation of the first order reaction is represented as Eq. (15), then the dependence $\lg C = f(t)$ is linear. The linearity of this dependence constructed from the experimental data (the lines in Figs. 4-5) allows us to conclude that this reaction (the Fe₃O₄ nanoparticles dissolution in the acid media) is of the first order. The rate constant of the reaction in this case is determined according to Eq. (16):

$$\lg C = \lg C_0 - \left(\frac{k}{2.3} \right) t \quad (15)$$

$$\text{tg } j = -\frac{k}{2.3} \quad (16)$$

where j is a slope of the dependence $\lg C = f(t)$.

In our case, when the dependences $-\lg C_{(Fe^{3+})} = f(t)$ are plotted near each other and have practically the same slope, we can assume:

– for the first interval of kinetic curves (Fig. 4) in the model solution of pH = 1.8: $-\text{tg } \varphi = -\lg C_{(Fe^{3+})} = -1.90$;
 $k_1 = -(2.3 \text{tg } \varphi) = -(2.3 \cdot (-1.90)) = 4.37$;

– for the second interval: $-\text{tg } \varphi = -\lg C_{(Fe^{3+})} = -0.04$;
 $k_2 = -(2.3 \text{tg } \varphi) = -(2.3 \cdot (-0.04)) = 0.09$;

– for the first interval of kinetic curves (Fig. 5) in the model solution of pH = 5.0: $-\text{tg } \varphi = -\lg C_{(Fe^{3+})} = -1.65$;
 $k_1 = -(2.3 \text{tg } \varphi) = -(2.3 \cdot (-1.65)) = 3.80$;

– for the second interval: $-\text{tg } \varphi = -\lg C_{(Fe^{3+})} = -0.03$;
 $k_2 = -(2.3 \text{tg } \varphi) = -(2.3 \cdot (-0.03)) = 0.07$.

So, the dissolution rate constants found by spectrophotometric, atomic-absorption and gravimetric methods, are close: for the solution of pH = 1.8 $k_1 = 4.37$ and $k_2 = 0.09$; for the solution with pH = 5.0 $k_1 = 3.80$; $k_2 = 0.07$. Therefore, the values found *via* different physico-chemical methods are valid and may be used to determine the process rate.

The analysis of the experimental (Figs. 4-5) and the calculated data shows that in the medium with the higher acidity (pH = 1.8) the dissolution rates of the near-surface (k_1) and bottom (k_2) layers of the Fe₃O₄ nanoparticles are greater by 1.15 and 1.29 times, respectively, in comparison with the corresponding dissolution rates of the particles in the medium with the lower acidity (pH = 5.0).

Thus, in a high-acid medium the process of Fe₃O₄ nanoparticles dissolution is more intensive by 1.22 times compared with that in a low-acid medium. In other words,

the decrease in the medium acidity leads to the retardation and deterioration of the Fe_3O_4 nanoparticles dissolution.

3.2. Effect of Acid Medium on the Physico-Chemical State on the Surface of Fe_3O_4 samples

The specific character of the physico-chemical and magnetic properties of the small particles, Fe_3O_4 in particular, is caused by the size and shape of the particles, as well as the morphology of the near-surface layer. We must consider the bevel geometry of the open surface of Fe_3O_4 particles, its structural and morphological defects (angles, exacerbations, polyatomic projections).

Evaluation of the state and thickness of the magnetic excited a near-surface layer of Fe_3O_4 nanoparticles under the influence of acid medium simulating the upper gastrointestinal tract will allow to predict the physical and chemical behavior of Fe_3O_4 nanoparticles themselves and as a part of supramolecular assemblies with the biopolymer molecules of food systems.

The electronic micrograph and the distribution diagram of Fe_3O_4 nanoparticles in the sample 1 are shown in Fig. 6.

Fe_3O_4 nanoparticles synthesized *via* chemical coprecipitation (condensation) have the single morphology (Fig. 6a). The shape of Fe_3O_4 nanoparticles is not clearly expressed and is perceived as a spherical one. In addition, the particles aggregation with the clusters formation is observed. This fact provides the closure of the magnetic flux and can be explained by the absence of an external magnetic field during the electron microscopic researches. We can notice that the clusters consist of small particles and the boundaries of each particle are clearly visible.

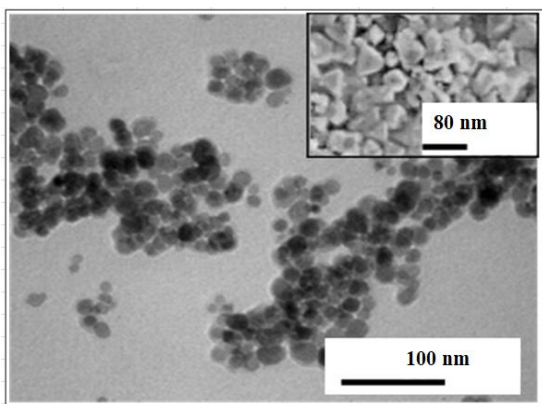
On the basis of obtained photos the particles distribution according to the diameter was calculated (Fig. 6b). The distribution function was found to be sufficiently

narrow and symmetric, which characterizes the system of the synthesized Fe_3O_4 nanoparticles as a homogeneous one with a low degree of polydispersity. The established average particle size of Fe_3O_4 is 78 nm.

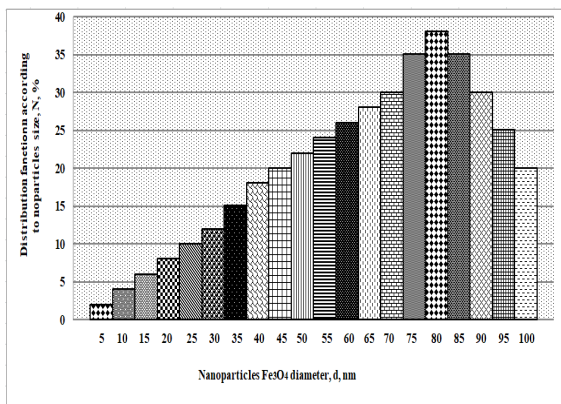
The spinel structure of Fe_3O_4 nanoparticles in the experimental sample 1 was confirmed by XRD. Fig. 7 shows the full profile X-ray diffraction pattern of the experimental sample 1. One can see that the synthesized Fe_3O_4 nanoparticles belong to the ferros spinels [35, 39-43]. The name "spinel structure" comes from the name of the MgAl_2O_4 mineral which is crystallized in the cubic system (Fig. 8) [39].

Elementary cell of the system has eight molecules of MeFe_2O_4 . The relatively large oxygen ions form a face-centered cubic lattice. The densely packed cubic structure has 8 tetrahedral (A-nodes) and 16 octahedral (B-nodes) cavities (places), which are occupied by the metal ions. Depending on the distribution of di- and trivalent ions according to sublattices there are normal, inverse and mixed spinels. In the inverse spinel structure the bivalent ions are located in the octahedral positions (one per unit) and the trivalent ions are equally divided between the octahedrons and tetrahedrons (one per unit in the position of a certain type).

The obtained results (Fig. 7) and calculations show that the main bands correspond to Fe_3O_4 with the inverse spinel structure: Fe(II) cations occupy B-nodes, and Fe(III) ions are distributed between A - and B-nodes. Hence, the refined formula for Fe_3O_4 particles is $\text{Fe}^{3+}[\text{Fe}^{3+}\text{Fe}^{2+}]\text{O}_4^{2-}$; the crystal lattice parameter is 0.83716(4) nm, while for an ordered and stoichiometric Fe_3O_4 the crystal lattice parameter is 0.83952(2) nm. However, in contrast to the conventional magnetite [41, 42], there is a decrease in the *d*- and *a*-parameters of an elementary cell in Fe_3O_4 nanoparticles of the sample 1 indicating a crystal lattice compression in the synthesized nanoparticles [39-42].



a)



b)

Fig. 6. The electronic micrograph (a) and distribution diagram (b) of Fe_3O_4 nanoparticles in the experimental sample 1 according to the size

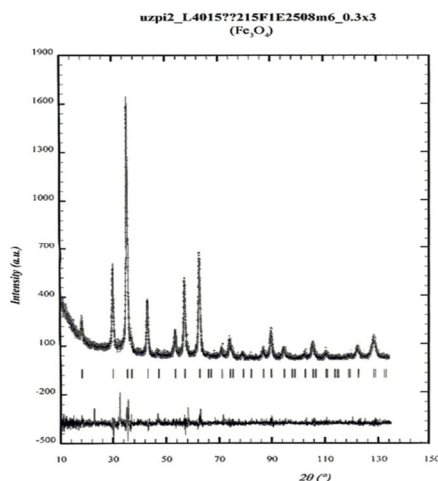


Fig. 7. X-ray diffraction pattern of the experimental sample 1 – synthesized Fe₃O₄ nanoparticles

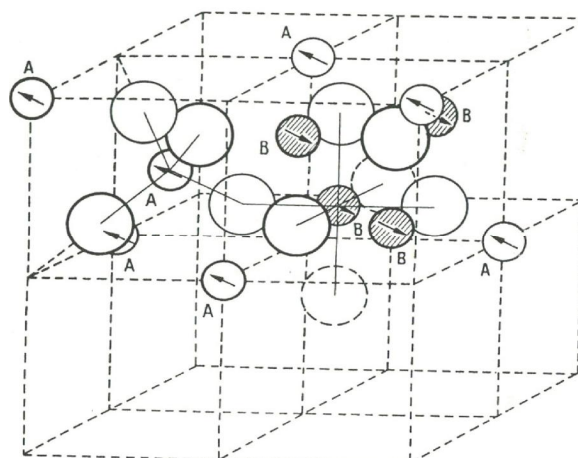
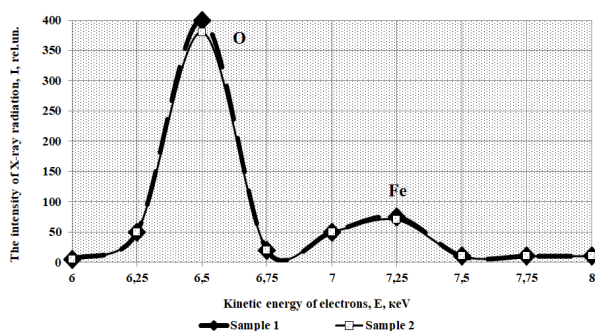
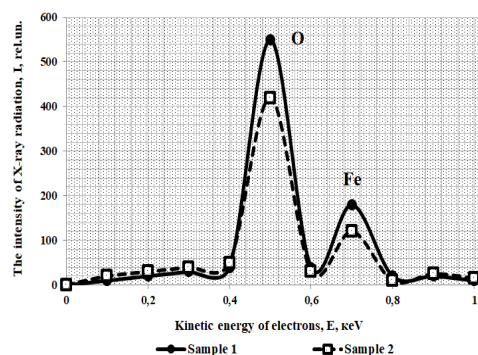


Fig. 8. Fe₃O₄ crystal structure (two octants of the spinel structure)



a)



b)

Fig. 9. The spectra of characteristic X-rays radiation from the volume (a) and surface (b) of Fe₃O₄ particles in the experimental samples 1 and 2

The broadening of bands on the X-ray diffraction pattern (Fig. 7) indicates an insignificant intensity of Fe₃O₄ particles crystal structure. This affects the physico-chemical properties of Fe₃O₄ nanoparticles, namely increases their surface activity and reactivity, e.g. the ability to interact with the food systems biopolymers and to form the colloidal solutions. The established effect (approximately 5 %) is concerned with a small deficit of Fe³⁺ and Fe²⁺ cations in both tetrahedral and octahedral positions. But in general, this effect can be very important and valuable for the biopolymer matrices modification and the colloidal systems stabilization. Three quite clear bands are also observed in Fig. 7, indicating the presence of an insignificant amount of a substance with a high-symmetric crystal lattice which can be identified as an impurity. When analyzing the impurities the following substances were supposed to be present: FeO (card. 20-138), Fe₂O₃ (card. 29-749), Fe(OH)₃ (card. 20-127), FeO(OH) (goethite, card. 29-713) and Fe₃O₄ (card. 28-162). According to the Rietveld refinement it was

established that the first four phases on the X-ray diffraction pattern are absent and the mass fraction of the fifth phase (Fe₃O₄) in the experimental sample is 95 ± 2 %.

Using the Sherrer equation [35] the average size of the synthesized Fe₃O₄ nanoparticles was also determined:

$$L = \frac{0.9l}{B \cos q} \quad (17)$$

where L is the size of Fe₃O₄ nanoparticle, nm; B is the half-width at the peak height, rad or $2q$; q the angle corresponding to the diffractational maximum at $2q$; l is the wavelength of the X-ray radiation, nm.

According to the calculation results the average size of the synthesized particles of Fe₃O₄ powder was ~78 nm.

The spectra of characteristic X-rays radiation from the volume and surface of Fe₃O₄ particles in the experimental samples 1 and 2 are shown in Fig. 9.

The analysis of the spectra (Fig. 9) shows no changes in the iron content in the volume of Fe_3O_4 nanoparticles for both experimental samples (Fig. 9a). For the near-surface layer the content of Fe and O_2 in the sample 2 (Fig. 9b) decreases by 35 and 20 %, respectively, compared to the original sample 1.

According to the previous researches [43–45] and the “shell model” [43] the structure of Fe_3O_4 nanoparticles consists of the total diameter of the solid particle (d) and the thickness of the surface layer (δ) with the “non-collinear” physico-chemical, in particular the magnetic structure. Schematically the structure is shown in Fig. 10.

Under the action of the medium of $\text{pH} = 1.8$ the part of near-surface layer of a certain thickness (δ') is removed. The value δ' was calculated using the obtained experimental data and a value corresponding to the maximum effect of the Fe_3O_4 nanoparticles dissolution (Table 3) with Fe^{3+} cations concentration of $6.40 \cdot 10^{-3} \text{ mol/dm}^3 = 3.6 \cdot 10^{-1} \text{ g/dm}^3$.

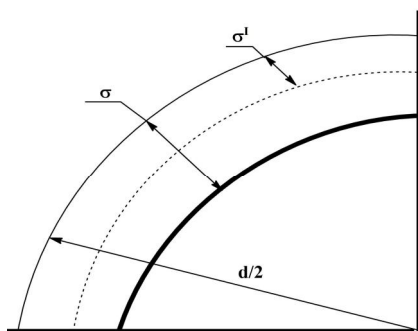


Fig. 10. Schematic structure of Fe_3O_4 nanoparticles of a certain diameter

Hence, the weight of Fe^{3+} cations passed into the solution (per 100 ml of HCl solution) in the working volume is:

$$m_{\text{Fe}_{\text{sol}}} = 3.6 \cdot 10^{-2} \text{ g} \quad (18)$$

According to the elemental composition micro-analysis of the near-surface layer (Fig. 9b) the initial weight of Fe in the near-surface layer decreased by 35 % with the loss of $3.6 \cdot 10^{-2} \text{ g}$ is:

$$m_{\text{Fe}_{\text{sol}}} = \frac{3.6 \cdot 10^{-2}}{0.35} = 1.03 \cdot 10^{-2} \text{ g} \quad (19)$$

Based on the sample weight used in the experiments $m_w = 2.5 \text{ g}$, the Fe weight in it is:

$$m_{\text{Fe}_{\text{total}}} = 2.5 \cdot 60.3 = 1.51 \text{ g} \quad (20)$$

The mass fraction of Fe passed into the solution is:

$$w_{\text{Fe}_{\text{sol}}} = \frac{3.6 \cdot 10^{-1}}{3} \cdot 100\% = 12\% \quad (21)$$

The mass fraction of Fe assumed to form the near-surface layer of the particle is:

$$w_{\text{Fe}_{\text{ass}}} = \frac{0.12}{3} \cdot 100\% = 4\% \quad (22)$$

The share of Fe passed from the near-surface layer into the solution is $4.0/12 = 0.333$ or 33.3 %

The above calculations were confirmed by the researches on the surface layer structure of the synthesized Fe_3O_4 particles in the samples 1 and 2 using the method of the nuclear gamma-resonance (Mössbauer) spectroscopy [44, 45] and nuclear magnetic resonance (NMR) on ^{57}Fe nuclei [46–52].

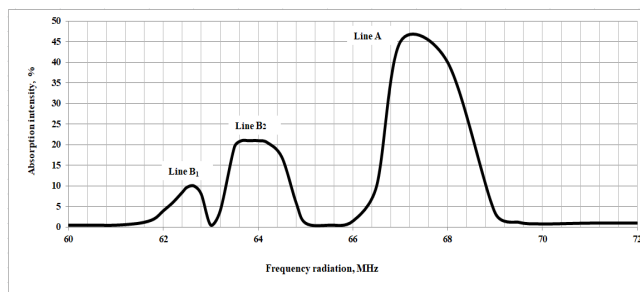
In Figs. 11 and 12 the results of acid medium effect on the NMR spectra of Fe_3O_4 sample are shown.

When comparing the NMR spectra of the synthesized finely dispersed Fe_3O_4 nanoparticles with monocrystalline samples of Fe_3O_4 at 298 K we observe the coincidence of resonance bands with some expansion of the resonance lines in the spectra of Fe_3O_4 nanoparticles. This effect is probably due to the increase in the local magnetic fields distribution surface on resonant nuclei since the crystal lattice and the magnetic structure of the nanoparticles are less perfect than those of monocrystalline samples [46, 47].

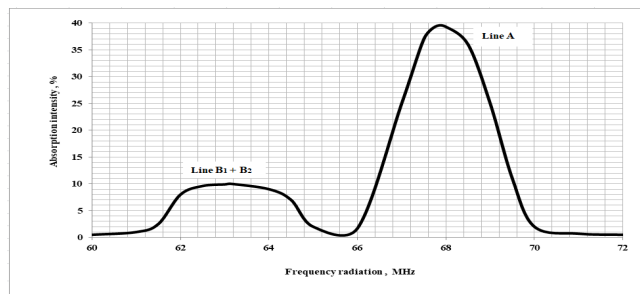
A strong signal in the region of 67.75 MHz (Line A) corresponds to the magnetite (Fe_3O_4) resonance, lines of lower intensity (Lines B_1 and B_2 – 62.63 and 63.66 MHz, respectively) correspond to the maghemite (Fe_2O_3) resonance [47–50]. After treatment of the samples 2 and 4 with the chloride acid the intensity of all triplet bands (samples 2, 4) is reduced in comparison with the initial samples (samples 1 and 3): Lines B_1 and B_2 – by 42–43 %; Lines A – by 8–12 %. For the sample 2 the confluence of Lines B_1 and B_2 is observed with the formation of one broad band the intensity of which is lower than that of Lines B_1 and B_2 . It means that the Fe_3O_4 nanoparticles dissolution, associated with a violation of the structural composition stoichiometry and exchange interactions of Fe–O–Fe bonds on the surface and near-surface layers, predictably affects the “non-collinear” magnetic structure of the near-surface layer and the physico-chemical characteristics on the whole, which should be investigated in future.

The spin echo method for all samples was used additionally to determine ^{57}Fe NMR at 298 K. The relaxation times were measured and the magnetic field effect on the spin echo signal amplitude was defined. The results are shown in Fig. 13.

The signal of the spin echo was detected in the same frequency region as for an ordinary iron [51, 52]. The amplitude of the echo in finely dispersed Fe_3O_4 samples (samples 1 and 2) is much weaker than that in the monocrystalline samples of Fe_3O_4 (samples 3 and 4). To increase the signal/noise ratio a significant increase in the number of accumulation was required.

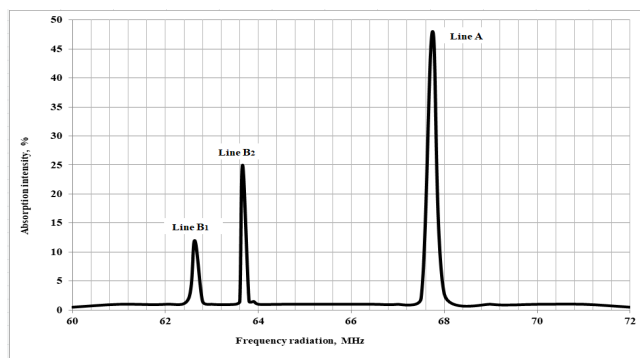


a)

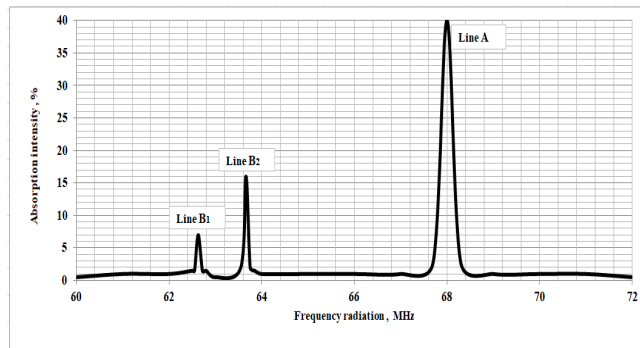


b)

Fig. 11. NMR ^{57}Fe spectra of the finely dispersed Fe_3O_4 samples: initial sample 1 (a) and acid-treated sample 2 (b)



a)



b)

Fig. 12. NMR ^{57}Fe spectra of monocrystalline Fe_3O_4 samples: initial sample 1 (a) and acid-treated sample 2 (b)

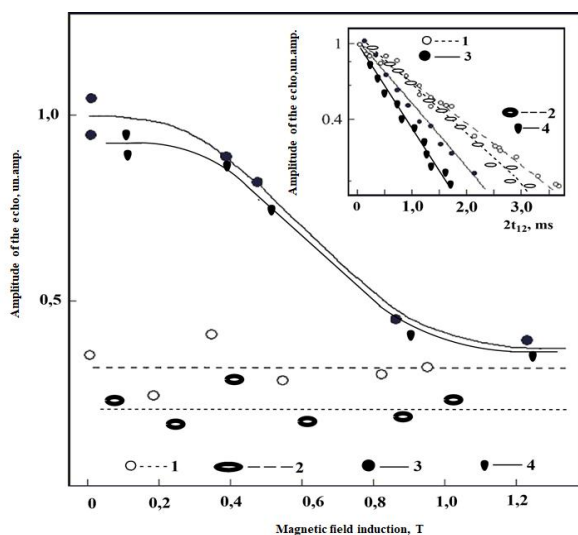


Fig. 13. ^{57}Fe spin echo amplitude vs. external magnetic field at 298 K for the experimental samples 1–4. Inset: spin echo amplitude vs. doubling time between the excitation pulses at 298 K

It is evident from Fig. 13 that the spin echo spectra of finely dispersed and monocrystalline Fe_3O_4 are similar, though the time of transverse nuclear relaxation (Fig. 13, inset) for the samples 1 and 2 is by 1.36 times (1.4 ms for the sample 1 and 1.9 ms for the sample 2) and 1.77 times larger (0.9 ms for the sample 1 and 1.6 ms for the sample 2) than for the samples 3 and 4. Moreover, the dissolution

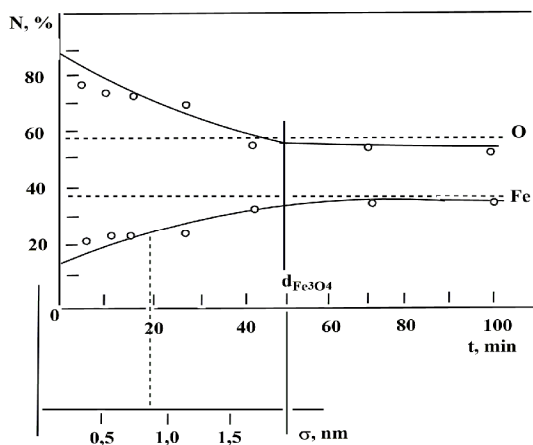


Fig. 14. Change in the elemental composition of the sample 2 depending on the dissolution time

When investigating the physico-chemical, functional and technological properties of Fe_3O_4 nanoparticles the value of the near-surface layer thickness is important. Taking into account that the particles are three-dimensional objects, the surface atoms, depending on the particle size,

of the near-surface layer in the samples 2 and 4 contributes to the increase in the transverse nuclear relaxation time compared with the initial samples 1 and 3. With the increase in the induction value the signal for monocrystalline samples (3 and 4) rapidly decreases and practically is not changed for the finely dispersed samples (1 and 2). This effect is explained by the fact that the main source of the nuclear spin system response is the domain boundaries for the monocrystalline samples, and domains for the finely dispersed nanoparticles [51].

The relaxation time of nuclear transverse is larger for the samples 1 and 2 compared with that for the samples 3 and 4 (Fig. 13). It is apparent in the decrease of echo signal, characterizing the superparamagnetic nature of the ferromagnetic moment motion, though this effect is not observed for the Fe_3O_4 nanoparticles. So, the fixation of the individual crystallites moments takes place, for instance due to the close location of the Fe_3O_4 nanoparticles in the agglomerates formed by them. However, the interaction between nanoparticles in agglomerates is weak, since the Fe_3O_4 particles are separated by an oxide shell – the main component of the near-surface layer.

The present and previous experiments [44, 45, 51, 52] show the change in the elemental composition of the near-surface layer of the Fe_3O_4 nanoparticles in the acid medium (Fig. 14). 0.333 % of the curve corresponds to the thickness of 0.85 nm. These data are confirmed by the results of transmission electron microscopy presented in Fig. 15.

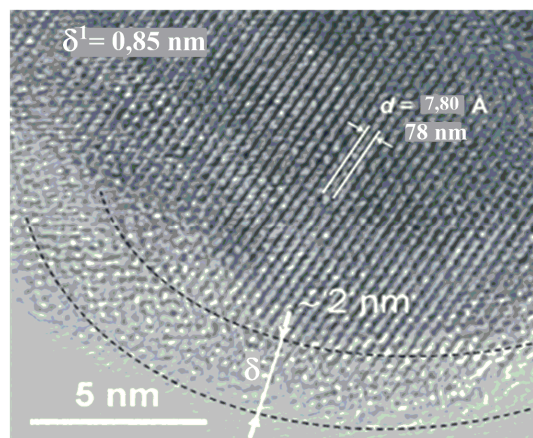


Fig. 15. TEM photos of the synthesized Fe_3O_4 nanoparticles (sample 1)

can occupy a significant percentage of the particle total volume. Not only open surface is included, but the structurally defective near-surface layers as well. The greater the open surface effect, the smaller the crystal dimensions. According to the postulates of the “shell

model” [43-45], the main parameters of the particle size are the total diameter of the solid particle ($d = 78$ nm) and the thickness of the near-surface layer ($\delta = 2.0$ nm) with the “non-collinear” magnetic structure (Fig. 15). The thickness is a function of many parameters. The method and conditions for the particles synthesis, as well as the conditions for their use play a decisive role. According to various studies [44, 45] for the Fe₃O₄ particles the total thickness of the near-surface layer is 0.8–2.0 nm. When the particles with $d \sim 78$ nm and the near-surface layer thickness of ~ 2.0 nm (Figs. 6b and 15) are treated with an acid medium (pH = 1.8), 0.85 nm of the particle is removed. In our case, the volume fraction of the structurally defective surface is 26 % of the particle total volume.

4. Conclusions

The process of the synthesized Fe₃O₄ particles dissolution in media of pH = 1.8–5 was studied and the solubility of these particles was found to be limited. The kinetic equations and rate constants of dissolution reactions of Fe₃O₄ particles in media of pH = 1.8 and pH = 5.0 were determined.

The obtained data can be used to evaluate the near-surface layer activity of metal nanoparticles and metal oxides in acid media of biological and technological objects as an additional mineral source of easily digestible iron Fe(II). The mechanism of the acid medium effect on the state of the near-surface layer of Fe₃O₄ nanoparticles was determined by a scanning electron spectroscopy, X-ray diffraction analysis and nuclear magnetic resonance. The thickness of the surface layer and its volume fraction, which is soluble in acid media, were established. In our case, the volume fraction of the structural-defect surface is 26 % of the particle total volume, *i.e.* the thickness of the near-surface layer ~ 2.0 nm, and 0.85 nm was dissolved.

These experimental data are of interest in a variety of technologies for predicting, correcting and forming the functional and technological properties of Fe₃O₄ nanoadditive in technological compositions. The obtained results will allow to simulate the dissolution process of the metals and their oxides nanoparticles in an acid media; processes of their digestion in the gastrointestinal tract; physico-chemical processes in biotechnologies when using nanoparticles of this type.

It should be noted that further researches of the Fe₃O₄ nanoparticles dissolution in the neutral and alkaline media is of great interest.

References

- [1] Ambrozevich E.: Pishchev. Ingrid. Syrye i Dobavki, 2005, **1**, 30.
- [2] Spirichev B., Shatnyuk L., Poznyakovskiy V.: Pishchev. Prom., 2003, **3**, 10.
- [3] Ostapchuk Yu.: Balansy ta Spozhyvannia Osnovnykh Produktiv Kharchuvannia Naseleenniam Ukrainy: Statystychnyi Zbirnyk za 2004 rik. Kyiv 2005.
- [4] Yliukha N., Barsova Z., Kovalenko V., Tsykhanovskaia Y.: Vost.-Eur. Zh. Peredov. Tekhnol., 2010, **6**, 32.
- [5] Alexandrov A., Tsykhanovska I., Evlash V. *et al.*: East.-Eur. J. Adv. Technol., 2018, **2**, 70. <https://doi.org/10.15587/1729-4061.2018.126358>
- [6] Alexandrov A., Tsykhanovska I., Evlash V. *et al.*: Eureka Life Sci., 2017, **5**, 45. <https://doi.org/10.21303/2504-5695.2017.00431>
- [7] Evlash V., Pogozhikh N., Akmen V.: Nauchnye Osnovy Tekhnologiy Pishchevykh Produktov Antianemicheskoy Napravlennosti so Stabilizirovannym Gemovym Zhelezom. Khdukht, Kharkiv 2016.
- [8] Specification for Food Additives and Recipes, 2013. <http://specin.ru>
- [9] Beriain M., Gómez I., Ibáñez F. *et al.*: Chapter 1 - Improvement of the Functional and Healthy Properties of Meat Products [in:] Holban A., Mihai A. (Eds.), Food Quality: Balancing Health and Disease. Academic Press, 2018, 1-74. <https://doi.org/10.1016/B978-0-12-811442-1.00001-8>
- [10] Domoroshchenkova M., Demyanenko T., Kamysheva I. *et al.*: Oliyno-Zhyrovyi Komplex, 2007, **4**, 24.
- [11] Novinyuk L.: Pishchev. Ingrid. Syrye i Dobavki, 2007, **1**, 40.
- [12] Lai W., Khong N., Lim S. *et al.*: Trends Food Sci. Technol., 2017, **59**, 148. <https://doi.org/10.1016/j.tifs.2016.11.014>
- [13] Shishkov Yu.: Pishchev. Prom., 2004, **12**, 92.
- [14] Renziaeva T., Pozniakovskiy V.: Khranenie i Pererabotka Selhozsya, 2009, **7**, 14.
- [15] De Romana D., Brown K., Guinard J.: J. Food Sci., 2002, **67**, 461. <https://doi.org/10.1111/j.1365-2621.2002.tb11429.x>
- [16] Lyublinskiy S., Lyublinskaya I., Chernyayev S., Markov M.: Molochn. Prom., 2004, **5**, 5.
- [17] Lyublinskiy S., Dubina S.: Molochn. Prom., 2003, **5**, 10.
- [18] Paglarini C., Furtado G., Biachi J. *et al.*: J. Food Eng., 2018, **222**, 29. <https://doi.org/10.1016/j.jfoodeng.2017.10.026>
- [19] Ramachandraiah K., Choi M.-J., Hong G.-P.: Trends Food Sci. Technol., 2018, **71**, 25. <https://doi.org/10.1016/j.tifs.2017.10.017>
- [20] Budryn G., Zaczyńska D., Oracz J.: LWT, 2016, **73**, 197. <https://doi.org/10.1016/j.lwt.2016.06.019>
- [21] Evlash V., Pohozhykh N., Vynnykova V.: Vost.-Eur. Zh. Peredov. Tekhnol., 2004, **2**, 22.
- [22] Saini R., Nile S., Keum Y.: Trends Food Sci. Tech., 2016, **53**, 13. <https://doi.org/10.1016/j.tifs.2016.05.003>
- [23] Cao M., Li Z., Wang J. *et al.*: Trends Food Sci. Tech., 2012, **27**, 47. <https://doi.org/10.1016/j.tifs.2012.04.003>
- [24] Peters R., Bouwmeester H., Gottardo S. *et al.*: Trends Food Sci. Tech., 2016, **54**, 155. <https://doi.org/10.1016/j.tifs.2016.06.008>
- [25] Gaucheron F.: Trends Food Sci. Tech., 2000, **11**, 403. [https://doi.org/10.1016/S0924-2244\(01\)00032-2](https://doi.org/10.1016/S0924-2244(01)00032-2)
- [26] Gupta C., Chawla P., Arora S. *et al.*: Food Hydrocolloid, 2015, **43**, 622. <https://doi.org/10.1016/j.foodhyd.2014.07.021>
- [27] Abukhader M.: Nutr. Health, 2018, **24**, 103. <https://doi.org/10.1177/0260106018767686>
- [28] Egbi G., Ayi I., Saalia F. *et al.*: Food Nutr. Bull., 2015, **36**, 264. <https://doi.org/10.1177/0379572115596253>
- [29] Iliukha M., Barsova Z., Timofeieva V., Tsykhanovska I., Vedernykova I.: Khim. Prom. Ukrainy, 2009, **5**, 32.
- [30] Iliukha M., Barsova Z., Timofeieva V. *et al.*: Ukr. Pat. 54284, Publ. Nov. 10, 2010.
- [31] Derzhavna Farmakopiia Ukrainy. http://sphu.org/wp-content/uploads/2016/12/Content_2izd_1dop.pdf

- [32] Sayenko Ye.: Analiticheskaya Khimiya. Feniks, Rostov-na-Donu, 2018.
- [33] Boki G., Poray-Koshits M.: Rentgenostrukturnyy Analiz. MGU, Moskva 1964.
- [34] Shpak A., Horbyk P., Chekhun V. et al.: Physico-Khimiya Nanomater. i Supramol. Structur, 2007, **1**, 45.
- [35] Levitin nE., Vedernikova I., Onoprienko T., Tsykhanovska I.: Pharmacom, 2007, **1**, 61.
- [36] Rao B., Kumar A., Rao K.: J. Optoelectron. Adv. Mat., 2006, **8**, 1703.
- [37] Olkhovik L., Sizova Z., Shurina E., Kamzin A.: Physica Tverdogo Tela, 2005, **47**, 1261.
- [38] Ershov Yu.: Mekhanizmy Toksicheskogo Deystviya Neorganicheskikh Soyedineniy. Meditsina, Moskva 1989.
- [39] Belov K.: Fizika i Khimiya Ferritov. MGU, Moskva 1973.
- [40] Lu A., Salabas E., Schuth F.: Angew. Chem. Int. Edit., 2007, **8**, 1222. <https://doi.org/10.1002/anie.200602866>
- [41] Fertman V.: Magnitnyye Zhidkosti – Estestvennaya Konvektsiya i Teploobmen. Nauka i Tekhnika, Minsk 1978.
- [42] Dikiy N., Medvedeva E., Fedorets I et al.: Visnyk Kharkiv. Univ., 2009, **859**, 89.
- [43] Coey J., Khalafalla D.: Phys. Stat. Sol. A., 1972, **11**, 229. <https://doi.org/10.1002/pssa.2210110125>
- [44] Koval A., Olkhovik L., Levitin E. et al.: Int. Conf. Functional Materials-2007. Ukraine, Crimea, Partenit 2007, 421.
- [45] Vedernyikova I.: Ukr. Med. Almanakh, 2011, **14**, 14.
- [46] Stepánková H., Görnert P., Chlan V. et al.: J Magn. Magn. Mater., 2010, **322**, 1323. <https://doi.org/10.1016/j.jmmm.2009.04.002>
- [47] Bastow T., Trinchi A.: Solid State Nucl. Magn. Reson., 2009, **35**, 25. <https://doi.org/10.1016/j.ssnmr.2008.10.005>
- [48] Lee S.: New J. Phys., 2006, **8**, 98. <https://doi.org/10.1088/1367-2630/8/6/098>
- [49] Procházka V., Stepánková H., Chlan V. et al.: Acta Phys. Polonica A., 2015, **127**, 514. <https://doi.org/10.12693/APhysPolA.127.514>
- [50] Kristan P., Chlan V., Stepánková H. et al.: J. Nanomater., 2013, **2013**. <https://doi.org/10.1155/2013/179794>
- [51] Matveyeva V., Bregan A., Volodin V. et al.: Zh. Tekhn. Phys., 2008, **34**, 34.
- [52] Kristan P., Chlan V., Stepánková H. et al.: Acta Phys. Pol. A, 2014, **126**, 138. <https://doi.org/10.12693/APhysPolA.126.138>

Received: September 25, 2018 / Revised: October 25, 2018 /
Accepted: December 22, 2018

КІНЕТИКА РОЗЧИНЕННЯ НАНОЧАСТИНОК Fe_3O_4 У КИСЛОМУ СЕРЕДОВИЩІ

Анотація. Вивчена розчинність дослідних зразків наночастинок Fe_3O_4 у кислому середовищі ($pH = 1,8-5,0$ 3,0 год.). Наведені кінетичні криві та результати розчинності Fe_3O_4 спектрофотометричним, гравіметричним та атомно-абсорбційним методами. Встановлено зростання розчинності Fe_3O_4 зі збільшенням кислотності середовища і часом перебування в ньому. Електронно-мікроскопічними, рентгено-структурними та ЯМР-дослідженнями встановлено вплив кислого середовища на фізико-хімічний стан поверхні дослідних зразків частинок Fe_3O_4 .

Ключові слова: наночастинок Fe_3O_4 , розчинність, кінетика, кисле середовище.